ADVANCED THERAPEUTICS
www.advtherap.com

Dual-Mode Vasodilator M119 Delivery to Hair Follicle via Dissolving Microneedle for Advanced Alopecia Treatment

*Youseong Kim, Yeong Chan Ryu, Hye Su Min, Huisuk Yang, Jeehye Nam, Chisong Lee, Daniel Junmin Um, Miji Kim, Paola Atzei, Rita de Brito Francisco, Reto Naef, Kang-Yell Choi, and Hyungil Jung**

Finasteride, the most widely used oral alopecia drug, shows several side effects such as hypoactive sexual dysfunction or depression, whereas the topical drug minoxidil demonstrates unsatisfactory efficacy. Thus, there is an increasing need for new alopecia drugs and alternative delivery systems for future alopecia treatment. Researchers have developed dissolving microneedle (DMN), a transdermal drug delivery system, which can be used with minimal invasion. However, DMN has limited application for the alopecia treatment owing to its unsuccessful implantation on the hairy scalp. Here, it is suggested that TOP-M119 (M119), a novel drug acting as a vasodilator in the scalp, and M119-loaded DMN with a specially designed shape can be used for the alopecia treatment. This M119-loaded DMN system is delivered using a newly designed applicator that supports patchless scalp implantation of DMN by microsized pillars designed to prevent accidental skin insertion. Enhanced hair follicle targeting drug delivery and superior alopecia treatment efficacy of specially designed shaped DMN and M119 has been demonstrated through in vitro and ex vivo studies. Moreover, M119-loaded DMN system shows enhanced in vivo efficacy in mouse skin and through expression markers related to hair growth, such as β-catenin, proliferating cell nuclear antigen, MECA 32, and versican.

1. Introduction

Alopecia is one of the most common disorders in modern society, which is caused by various factors such as genetic, hormones, autoimmune diseases, aging, and acute stress.[1] The most popular treatment is oral administration of the synthetic inhibitor of type-2 5α-reductase finasteride, which regulates the concentration of the androgenic hormone dihydrotestosterone.[2] However, it affects other androgen-dependent tissues by systemic effects, causing impaired reproductivity and hypoactive sexual dysfunction.[3] Furthermore, a recent study revealed that finasteride can cause adverse effect on mental health and increases the risk of suicidality and depression.[4,5]

To overcome these side effects caused by oral administration of finasteride, minoxidil, a topical alopecia drug, has been developed and widely used in clinics. However, minoxidil topical formulations experience difficulty in delivering the drug to the deep hypodermic region (>700 μm), where hair follicles are located, against the skin barrier.[6] Most topical drugs are absorbed in the stratum corneum and epidermis before it reaches the dermal papilla, which regulates hair inductivity such as hair follicle morphogenesis and regeneration.[7] In addition, since hair follicles grow in the anagen phase, they grow deeper in the skin layer, and it becomes more difficult for topical formulations to reach the growing hair follicles.[8] Considering drug delivery efficiency, topical route is not the best option for the alopecia treatment.

To meet patient compliance with improved efficacy for hair loss treatment, a hypodermic drug injection has been introduced.[9] However, hypodermic injections on the scalp cause bleeding and acute pain because several dozen injections are repeatedly administered. In addition, the depth of injection, which is important to deliver the drug to the hair follicle area, is not easily controlled and standardized due to manual administration of the injection by doctors.[10] To overcome the hypodermic injection limitations, a solid microneedle with a roller system was designed to make pores on the patient's scalp through rolling, thus improving the delivery efficiency of alopecia drug.[11] Although solid microneedles reduce pain to some extent, they cause

Y. Kim, Y. C. Ryu, H. S. Min, J. Nam, C. Lee, D. J. Um, M. Kim, K.-Y. Choi, H. Jung
Department of Biotechnology, Building 123
Yonsei University
50 Yonsei-ro, Seodaemun-gu, Seoul 03722, Republic of Korea
E-mail: hijung@yonsei.ac.kr
H. Yang, H. Jung
JUVIC
208Ho, 272, Digital-ro, Guro-gu, Seoul 08389, Republic of Korea
P. Atzei, R. de B. Francisco, R. Naef
TOPADUR Pharma AG
Grabenstrasse 11A, Schlieren 8952, Switzerland
K.-Y. Choi
CK Regeon Inc., Engineering Research Park
Yonsei University
50 Yonsei-ro, Seodaemun-gu, Seoul 03722, Republic of Korea

The ORCID identification number(s) for the author(s) of this article can be found under https://doi.org/10.1002/adtp.202200052

DOI: 10.1002/adtp.202200052

bleeding in patients similar to hypodermic injection. In addition, it simply delivers the drug through the channel made by the solid microneedle and thus still has difficulty in controlling the depth of injection and target delivery of the drug to the hair follicles. Further, solid microneedle systems still have some possible contamination issues and need to be applied by medical experts.

The ideal treatment for alopecia is such that the drug delivery is sufficient to stimulate hair follicles with minimal side effects. In this concept, dissolving microneedle (DMN), which can penetrate the skin and deliver a drug directly to the target area in a noninvasive and painless manner, has been widely utilized in recent years.[12] Because the DMN delivers the drug into hundreds of micrometers after skin insertion, it has the potential to reach the hair follicle region and thus standardize the alopecia treatment by continuous delivery of the drug to the target depth. Furthermore, the DMN does not leave needle waste and can be self-administered. These advantages make DMN a promising candidate for alopecia treatment.[13] DMN, which is commonly administered as patches, has its own limitation of difficulty in attaching the patches to a hairy scalp.[14] In addition to this, the conical shape of the DMN with most volume in the basal area has difficulty delivering an accurate amount of drug to the hair follicle area because the DMN is generally not entirely inserted into the skin through patches.[15] This problem worsens when DMN is applied for alopecia treatment on the scalp, where hairs act as obstacle for DMN insertion.

There have been several trials conducted to deal with the above limitations of the DMN. A microneedle applicator is one of the ways to overcome the penetration issue during scalp application.[16] The applicator shoots the microneedle array backward and provides sufficient speed and power for complete penetration of the microneedle into the hairy skin. Although an applicator successfully enhances the insertion, the fundamental problem in delivering a drug to hair follicles remains due to the conical shape of the DMN with most volume of the drug being accumulated at the base and not at the tip.[17] Therefore, complete penetration and new shape of the microneedle specialized for drug delivery to the hair follicle region are required. Nevertheless, current studies on microneedle for alopecia treatment had limited consideration on the applicator issue and microneedle shape for hair follicle drug delivery.

In this study, we propose a hair follicle-targeted standardized drug delivery system with depth control using a candlelit microneedle (CMN). Furthermore, we utilized a novel dual-mode of action PDE5 inhibitor/organic nitrate ester molecule named TOP-M119 (M119) because of its superior vasodilator drug efficacy than other vasodilators such as widely used sildenafil. The M119 releases nitric oxide (NO) through its intracellular bioactivation and locally inhibits PDE5 to stimulate blood perfusion in the scalp region. Because NO activates the soluble guanylate cyclase to synthesize cGMP and PDE5 inhibition prevents cGMP breakdown, an amplified cGMP by these mechanisms potentially ensues a strong vasodilation.[18] Therefore, M119 with its novel mechanism of action had the potential to enhance angiogenesis, as well as dilate the blood vessels in the scalp. Through in vitro experiments, we compared specialized target drug diffusion of CMN with a topical formulation and a conventional-shaped dissolving microneedle (conv-DMN) using the Nile red. Additionally, we analyzed M119's safety and efficacy in in vitro human platelets and human dermal papilla cell (hDPC) culture.[19] Further, in vivo animal studies were conducted in the 7 weeks old C57BL/6 female mice in the telogen phase, an appropriate model for alopecia.[20] We investigated in vivo efficacy focusing on hair shaft growth, anagen induction, epithelial growth of the skin, and hair follicle proliferation by enhanced blood circulation, and protein upregulation in DPC.

2. Result and Discussion

The schematic concept of the hair follicle targeting CMN is described and compared with a topical formulation and conv-DMN in **Figure 1**A. In topical formulation, most drug is trapped in the stratum corneum and epidermis, showing limited drug delivery to the hair follicle region, the target site for alopecia treatment. In contrast, drug delivery efficacy is increased in conv-DMN owing to the directly making a pore on the skin barrier. The major volume of the drug in conv-DMN, however, is located at the basal layer, restricting drug delivery to the upper layer of the skin and limiting delivery to the deeper dermis layer where hair follicles are located. The CMN, however, showed enhanced drug delivery to hair follicles and blood vessels compared with conv-DMN, despite being both microneedles successfully designed to overcome the skin barrier. This is due to the fact that CMN has a higher volume in the middle and at the tip, thereby releasing a comparatively higher amount of drug near the hair follicle region. In other words, the release of drugs is related to the concentration of loaded drugs around hair follicle as well as the morphology of microneedles. In the point that the release of drugs encapsulated in microneedles is related to the amount of drug loaded in microneedles' middle and tip where is located near hair follicle region. As a result, advanced hair induction and vascularization around the hair follicles were observed in the CMN group. This potential of hair follicle targeting delivery of CMN is also achieved through the use of an applicator that overcomes the hair obstacle for microneedle insertion without a patch, as shown in Figure 1B. In this application system, the finger force pushes each micropillar, which matches the corresponding individual CMN on the array, and thus successfully inserts each CMN into the scalp against the hair barrier. A newly designed stopper having the same length of the micropillar is designed to prevent accidental direct insertion of the micropillar into the skin. Furthermore, our new applicator does not leave rod-shaped remains above the skin, which might have otherwise reduced user compliance in our previous system.[10]

The fabrication process of CMN that included two major steps is shown in **Figure 2**A. The fabrication of the base layer and a candle-shaped convex layer with a sharp tip are the two consecutive steps reported in our previous study.[10] First, a viscous mixture of M119 and pharmaceutical grade hyaluronic acid (PHA) was dispensed on CMC film in contact with a sterilized metal plate with a constant gap of 300 μm and dried under a vacuum environment. After drying the droplets with an hourglass-like shape, the secondary droplets were dispensed on the base layer followed by centrifugation in a customized centrifugal lithography machine.[21] The secondary droplets after centrifugation and drying formed a sharp tip layer, resulting in a CMN with a candle-shaped conformation and a sharp tip for skin penetration, a wide head, and a narrow neck. Conv-DMN was also fabricated by

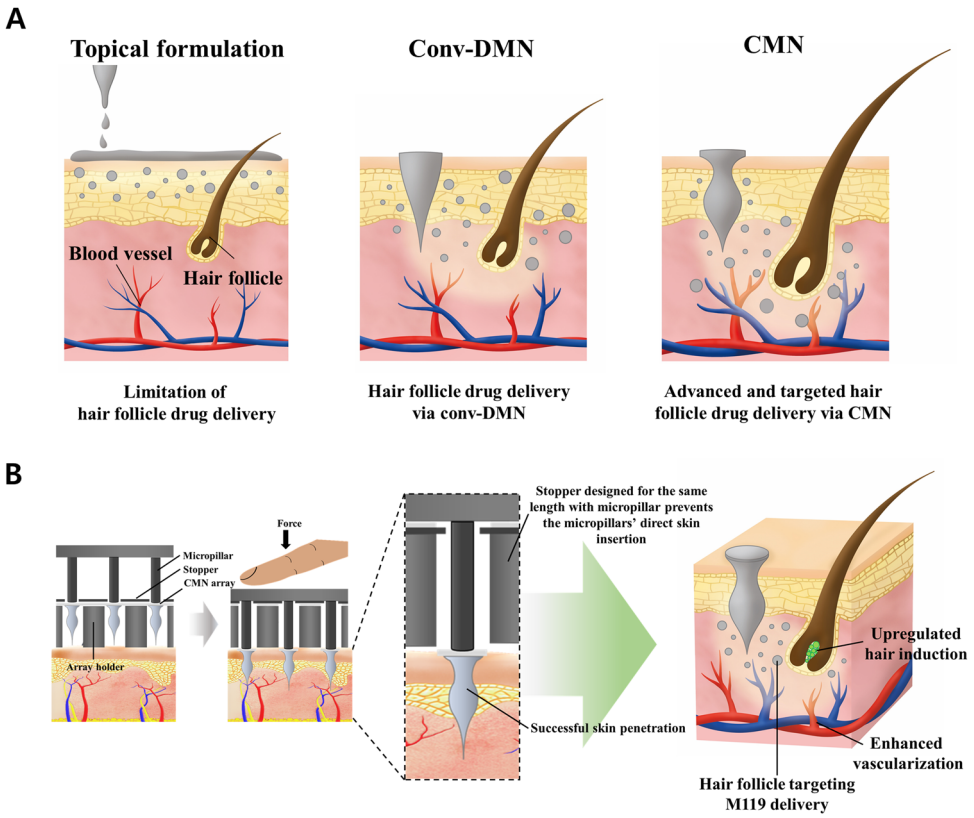

Figure 1. A) Schematic representation of drug diffusion from M119-loaded topical solution, conventional microneedle (conv-DMN), and candlelit microneedle (CMN) with the applicator in the hair follicle region. The hair follicle targeting delivery of M119 by CMN shows enhanced vascularization around the hair follicles and hair growth compared to the other groups. B) Successful penetration of CMN with the applicator without patches, and stopper prevents accidental insertion of micropillar into the skin. Successful hair growth was achieved by M119-loaded CMN with microneedle applicator system.

centrifugal lithography using M119 and PHA mixture. Bright field microscopic images and scanning electron microscope (SEM) images of M119-loaded conv-DMN and CMN having 700 μm height and sharp tips are shown in Figure 2B. The M119-loaded conv-DMN and CMN microneedle arrays are cut to 5 × 5 array size from originally produced array. Although the diameter of conv-DMN increased toward the base, the diameter of CMN, which had the widest part of the CMN at the head, increased, decreased, and increased again from the top to the bottom. This unique shape of CMN was specially designed for hair follicle targeted delivery of M119. In the SEM images of conv-DMN and CMN, we observed a smooth and streamlined surface. In Figure S1 in the Supporting Information, the average fracture force of conv-DMN was 0.38 N and CMN was 0.41 N ($n = 10$), indicating sufficient force for skin penetration.[11]

Because the sticky patch reduces the skin penetrating efficacy of the microneedle on the hairy scalp region, a microneedle applicator was utilized for CMN application. Figure 2C explains the components of the applicator system and their assembly in CMN. First, the CMN array was aligned to an array holder, which had holes corresponding to the CMN array, as shown in Figure S2 in the Supporting Information. After positioning the applicator above the skin, we pushed the micropillars of the applicator using the finger force. Next, the micropillars hit the bottom of the CMN, which then get separated and shot to the skin. Additionally, as shown in Figure 2C, the maximum movable distance of the micropillars was same as the length of the stopper. The micropillars pushed the individual CMN and moved forward until the length of the stopper was allowed. Using this mechanism, the stopper could prevent accidental skin insertion of the micropillars. This application system could deliver the CMN without a sticky patch, as shown in Figure 2D. In Figure 2D, the individual CMN (black arrowhead) shot from the CMN array was successfully inserted into the skin, and only the circle-shaped bottom (yellow dashed line) was observed. This implies that the CMN was completely inserted into the skin without a sticky patch by the applicator. Figure S3 in the Supporting Information clearly shows the shooting of a single CMN with a punctured CMN array using a micropillar. The diameter of the micropillar was 400 μm, and the bottom diameter of the shot CMN array was 600 μm. An image of the shoot and separated single CMN is shown in Figure 2E.

Conv-DMN and CMN were inserted into pig cadaver skin using the applicator and analyzed by optical coherence tomography (OCT) imaging (**Figure 3**A). Although trace patches are generally observed in OCT images, there were no patches detected in the OCT images, because both conv-DMN and CMN were separately inserted into the skin by the applicator without patches.[15] In addition to the skin insertion images shown in Figure 2D, the OCT images indicated successful individual penetration of conv-DMN and CMN using the applicator overcoming incomplete insertion

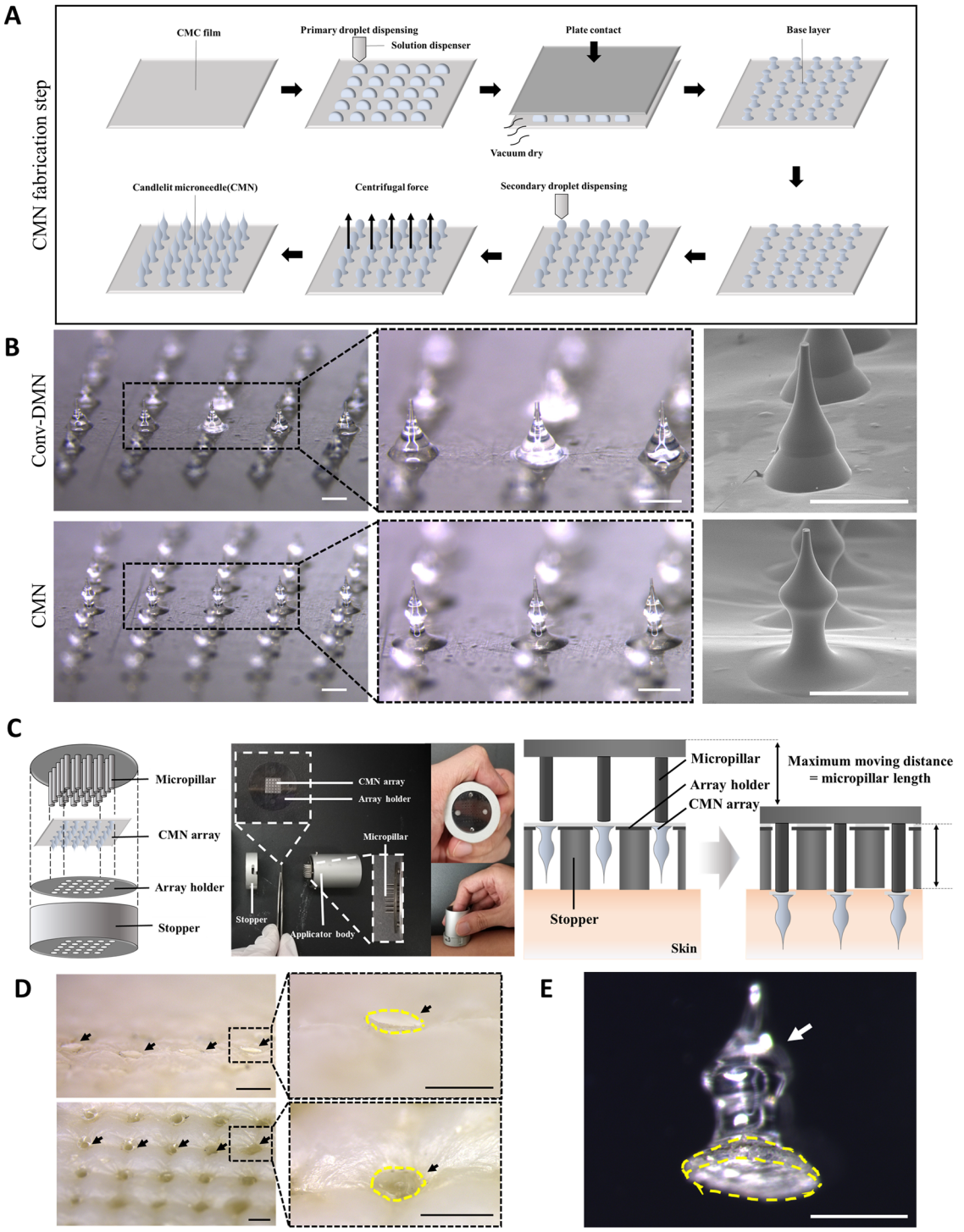

Figure 2. A) Schematic representation of fabrication steps of CMN. B) Morphological characteristics captured by bright field microscope and SEM of M119-loaded conv-DMN and CMN (scale bar, 500 μm). C) Assembly and usage of the applicator. Stopper restricts micropillar's moving distance to micropillar's own length. D) CMN array penetrated by the applicator with focused view of a single CMN. Arrowhead indicates CMN penetration in pig cadaver skin. Yellow dashed line indicates the bottom of the shot CMN (scale bar, 1 mm). E) Single CMN shot by the applicator. White arrowhead indicates CMN. Yellow dashed line indicates the bottom of the shot CMN (scale bar, 500 μm).

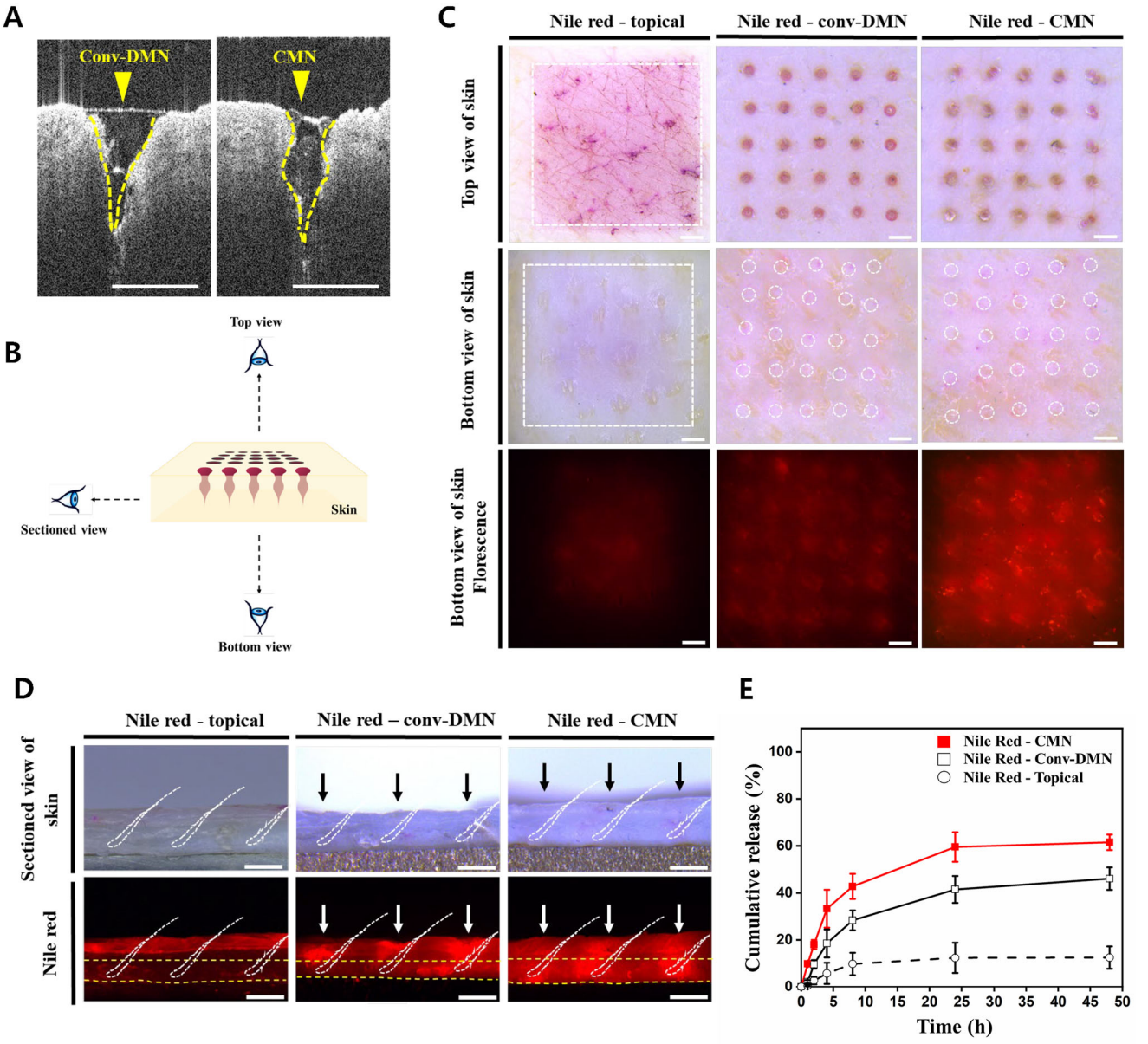

Figure 3. A) Optical coherence tomography (OCT) image of conventional microneedle and CMN for elucidation of the cross-sectioned skin penetration (scale bar, 500 μm). B) Schematic representation of the top view, bottom view, and sectioned view of the skin. C) Skin permeation analysis of Nile red topical formulation, Nile red conv-DMN, and Nile red CMN in pig cadaver skin. Bottom view fluorescence indicates lateral drug diffusion in the deep hypodermic region of skin. White dotted area represents the area where topical formulation, conv-DMN, and CMN are applied (scale bar, 1 mm). D) Cross-sectioned skin Nile red diffusion image indicates vertical drug diffusion in pig cadaver skin. Hair shafts are represented as white dashed line and hair follicles located in the hypodermic region, target site of alopecia drug, are represented by yellow-boxed area (scale bar, 1 mm). Stronger Nile red fluorescence intensity is detected around the hair follicles in the CMN group. E) Franz cell diffusion test of Nile red topical formulation, conv-DMN, and CMN for quantitative drug diffusion analysis. The cumulative release percentage of topical, conv-DMN, and CMN are 12.5 ± 4.7%, 41.5 ± 5.7%, and 59.5 ± 6.3%, respectively. Data are expressed as the mean ± SD ($n = 5$).

of the traditional microneedle patch. Nile red, which is known as a hydrophobic fluorescent dye, was chosen as the model drug of M119 in that the Nile red has similar log p value with hydrophobic compound M119 and is useful for visualizing and simulating hydrophobic drug dynamics in the skin.[22] Conv-DMN and CMN were fabricated using 0.1% w/v Nile red, as shown in Figure S4 in the Supporting Information. In the array of both groups, the height of microneedle was 700 μm and the distance between microneedles was 1.5 mm. We also prepared a topical formulation using 0.1% Nile red. The Nile red topical formulation, conv-DMN, and CMN were applied to pig cadaver skin using an applicator. After 24 h, we compared the fluorescence intensity of the bottom of pig cadaver skin to analyze Nile red permeation to the deeper skin area among the three groups. The viewpoint of our qualitative experiments is shown in Figure 3B. The top view of the skin showed the successful administration

Table 1. Recombinant human PDE5 enzymatic inhibition assay of M119 and its metabolites.

Compound	PDE5 IC50 [$\times 10^{-9}$ M]
M119	6.2
First metabolite of M119	0.64
Second metabolite of M119	0.15
Sildenafil	7.8

of both conv-DMN and CMN by the applicator; however, Nile red permeation of CMN was the highest among the three groups, as analyzed by the fluorescence intensity of the bottom view (Figure 3C). Because the thickness of pig cadaver skin was ≈1 mm, fluorescence intensity of the bottom view indicated that CMN released drug effectively into the deeper region of the skin than that of topical formulation and conv-DMN. In addition, the cross-sectioned Nile red diffusion images (Figure 3D) showed that topically administered Nile red was trapped in the upper region (stratum corneum and epidermis) of pig cadaver skin. We ascertained that conv-DMN and CMN groups diffused drug vertically inside pig cadaver skin, thus penetrating the upper region and releasing the drug directly inside the dermis layer. Interestingly, the CMN group showed better dermal drug delivery than that of the conv-DMN group. Vertical fluorescence intensity of the CMN group (yellow box, Figure 3D), which indicated hair follicle location, was markedly distinguished from the conv-DMN group. To support our qualitative comparison data (Figure 3C,D), we quantitatively analyzed the cumulative release profile of Nile red from topical formulation, conv-DMN, and CMN (Figure 3E). In 24 h of Franz cell test, the topical formulation, conv-DMN, and CMN groups showed cumulative release percentage of 12.5 ± 4.7%, 41.5 ± 5.7%, and 59.5 ± 6.3%, respectively. Thus, the CMN group showed 1.4-fold drug release in Franz cell compared to the conv-DMN group. Since both groups had same height of DMN and same loading amount of Nile red, this difference indicated that shape is a crucial factor that determines the quantitative release profile; CMN had ≈80% volume in the middle and tip regions of the conformation, whereas conv-DMN had a volume distribution of ≈50% in the middle and tip regions.[17]

Before conducting in vivo experiments, we strived to characterize M119 in enzymatic, cellular, and isolated organ level. Thus, we designed in vitro and ex vivo experiments by utilizing human platelets, hDPC, and mouse vibrissa. The platelets are known to contain both nitric oxide (NO) and PDE5 inhibitor targets in the relevant physiological levels. In addition to the cGMP measurement, we can also measure and correlate a functional response by a platelet adhesion assay. First, in an enzymatic assay using the human platelets to identify inhibitory concentration 50 (IC50), M119 (IC50 at 6.2×10^{-9} M) showed comparable potency to the reference PDE5 inhibitor sildenafil (IC50 at 7.8×10^{-9} M) to inhibit recombinant human PDE5 enzymatic activity (0.5×10^{-6} M cGMP substrate concentration) (**Table 1**). The lower IC50 value indicates higher inhibitor effect on PDE5. The M119's metabolites were detected from its bioactivation, first metabolite (IC50 at 0.64×10^{-9} M) and second metabolite (IC50 at 0.15×10^{-9} M) were more potent than sildenafil. Strikingly, M119 revealed more efficacious than sildenafil to elevate intracellular cGMP in platelets in spite of their comparable potency to inhibit PDE5 (**Figure 4**A). In general, it is known that the major two factors which upregulate cGMP concentration are PDE5 inhibition and NO-release promotion.[18] Therefore, this higher effect of M119 compared to sildenafil may be explained by the release of NO following bioactivated metabolism of M119. In other words, the NO-release and inhibition of PDE5 caused by M119 may result in drastically enhanced cGMP concentration than PDE5 inhibition alone. These findings strongly support the concept of M119 as a dual mode of action, NO-releasing PDE5 inhibitor.

Next, we analyzed the safety and efficacy of M119 in hDPC, which is a key cell with hair inductive properties. We compared in vitro cell viability and efficacy of M119 with those of minoxidil. In in vitro viability test using cell titer assay, the concentrations of M119 and minoxidil were diluted to 1/1000 scale of the in vivo concentrations.[23] M119 (30×10^{-9} M) and minoxidil (100×10^{-6} M) showed >80% viability (Figure 4B), which generally represents a safe condition.[18] Additionally, we performed real-time PCR test on M119-treated hDPC to validate the vasodilator activity of M119 by analyzing the mRNA level of vascular endothelial growth factor (VEGF), a key growth factor in hair growth (Figure 4C).[24] M119-treated group showed significantly enhanced VEGF expression level compared to the control and minoxidil groups. This indicated that M119 had superior vasodilating effect and hair growth potential than those of minoxidil. Furthermore, the protein level of proliferating cell nuclear antigen (PCNA), a proliferation marker in hDPC, was higher in the M119 group than in the control and minoxidil-treated groups (Figure 4D).[19]

After confirming the efficacy of M119 at the cell level, we further analyzed the efficacy of M119 at the isolated organ level under ex vivo conditions using mouse vibrissa, a stiff hair grown around the mouth of mice. As shown in Figure 4E, the vibrissa group treated with 30×10^{-9} M M119 showed the highest and most significant hair follicle elongation; moreover, 3×10^{-9} M M119 showed significant hair follicle elongation compared to the control and 100×10^{-6} M minoxidil-treated groups. In addition, the relative hair follicle elongation (%) was analyzed (Figure 4F); 30×10^{-9} M M119 showed ≈1.7-fold hair follicle elongation compared to the control group. From the mouse vibrissa elongation test, we could infer that M119 has a superior hair growth potential than the widely used minoxidil. Based on the hDPC and vibrissa test, we identified the efficacy of M119 at the cell and organ level. In the next step, we evaluated hair growth potential of CMN with an applicator system under in vivo conditions.

Prior to conducting in vivo test of M119-loaded CMN, we demonstrated that CMN could overcome the live mouse's hairy skin barrier and successfully penetrate the skin with the applicator within few seconds of application time, as shown in **Figure 5**A. Based on this result, we showed that our system could be applied to the skin regardless of the presence of hair. Next, in vivo efficacy of M119-loaded CMN was evaluated in 7 weeks old female mice at the telogen phase, four mice in each experimental group (Figure 5B). The images of all mice used in this experiment are shown in Figure S5 in the Supporting Information ($n = 4$ per group). We administered topical control and CMN control without the drug as negative control so we could not detect skin thickening for hair follicle development in hematoxylin and eosin (H&E) staining of Figure 5B. Next, 2% w/v topical minoxidil, widely selected as positive control in alopecia studies,[19]

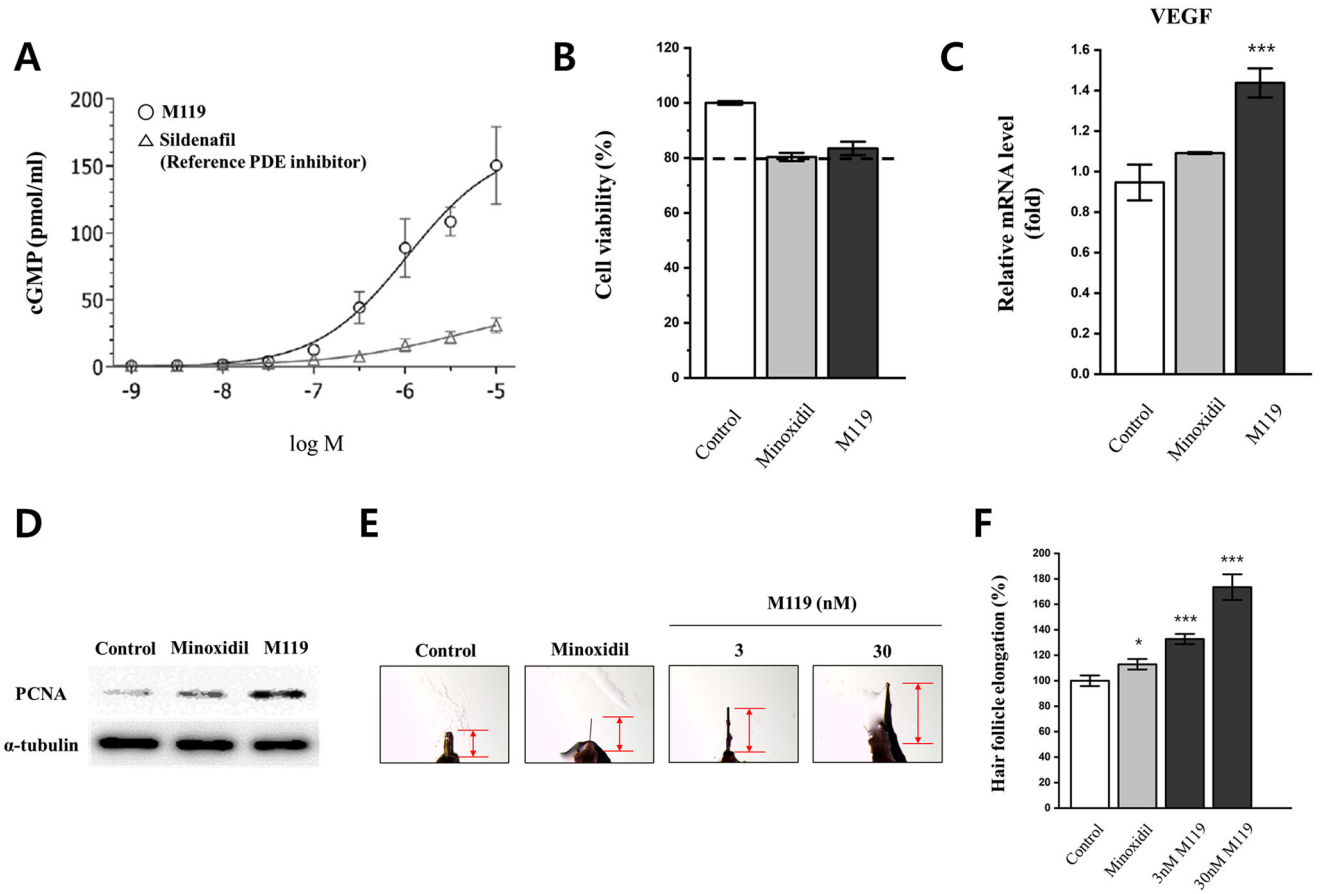

Figure 4. Effects of M119 on human platelets, human dermal papilla cell (hDPC), and vibrissa organ culture. A) Concentration-dependent effects of M119 on total cGMP in human platelets. The ELISA results (cGMP, pmol mL^{-1}) are from $n = 6$ (M119) and $n = 3$ (sildenafil) independent experiments, each performed in triplicate. Data are shown as the means ± SEM. B) Cell viability test of hDPC treated with DMSO control solution, 100×10^{-6} M minoxidil, and 30×10^{-9} M M119 for 24 h ($n = 6$). C) hDPC treated with control, 100×10^{-6} M minoxidil, and 30×10^{-9} M M119 for 48 h to determine VEGF expression. ***$p < 0.001$ compared to the control group. D) Proliferating cell nuclear antigen (PCNA) protein level in hDPC treated with DMSO, 100×10^{-6} M minoxidil, and 30×10^{-9} M M119, as analyzed by western blot. α-tubulin indicates loading control. E) Mouse vibrissa elongation by M119. The mouse vibrissa follicles were cultured with control, 100×10^{-6} M minoxidil, 3×10^{-9} M M119, and 30×10^{-9} M M119 for 6 days ($n = 6$). The red arrowhead indicates the length of vibrissa follicle. F) The length was measured after 6 days, and vibrissa follicle elongation rate was calculated as the difference between the experimental group and the control group considered 100% (scale bar, 500 μm). Data (B), (C), and (F) are expressed as the mean ± SD. *$p < 0.05$, **$p < 0.01$, ***$p < 0.001$.

0.002% w/w topical M119, and 2 μg (the same amount of drug loaded in topical formulation described in Figure S6, Supporting Information) M119-loaded conv-DMN and CMN were used in this study. Topical solutions were applied to the dorsal skin of all mice twice daily for 21 days, whereas drug-loaded conv-DMN and CMN were applied once every alternate day for 21 days. On day 21 (week 3), all experimental groups except the topical control and CMN control groups showed hair growth. In topical analysis, topical M119 showed superior hair growth compared to topical minoxidil, as analyzed by black-colored skin percentage, hair-bearing skin percentage, and hair follicle conversion from telogen-to-anagen phase. Furthermore, M119-loaded CMN showed more enhanced hair growth indices than those of M119-loaded conv-DMN.

During hair growth in mice, color of the dorsal skin changes from pink to black when hair follicles in the dorsal skin change from telogen to anagen state, which can induce hair growth. Thus, black-colored skin percentage and hair-bearing skin percentage indicate anagen conversion trend in the dorsal skin and actual hair growth from anagen state, respectively. In M119 topical formulation (Figure 5C), the black-colored skin percentage and the hair-bearing skin percentage (92.1 ± 3.0% and 61.0 ± 14.0%) were higher than those of minoxidil topical application (65.3 ± 22.3% and 38.4 ± 17.1%), respectively, on day 21. Because M119 induced improved vasodilation around hair follicles, which is one of the key factors beneficial for alopecia treatment, the results of anagen induction and hair growth were superior to those of the minoxidil group.

Moreover, we compared the efficacy of the M119-loaded CMN with that of M119-loaded conv-DMN (Figure 5D). The M119 CMN, which had 92.9 ± 11.2% of black-colored skin area and 90.7 ± 14.1% of hair-bearing skin area on day 21, showed more efficient hair growth than that of M119-loaded conv-DMN group with respective values as 82.5 ± 7.4% and 66.9 ± 17.5%. The M119-loaded CMN showed 1.35-fold larger hair-bearing area than that of M119-loaded conv-DMN. Surprisingly, similar trend

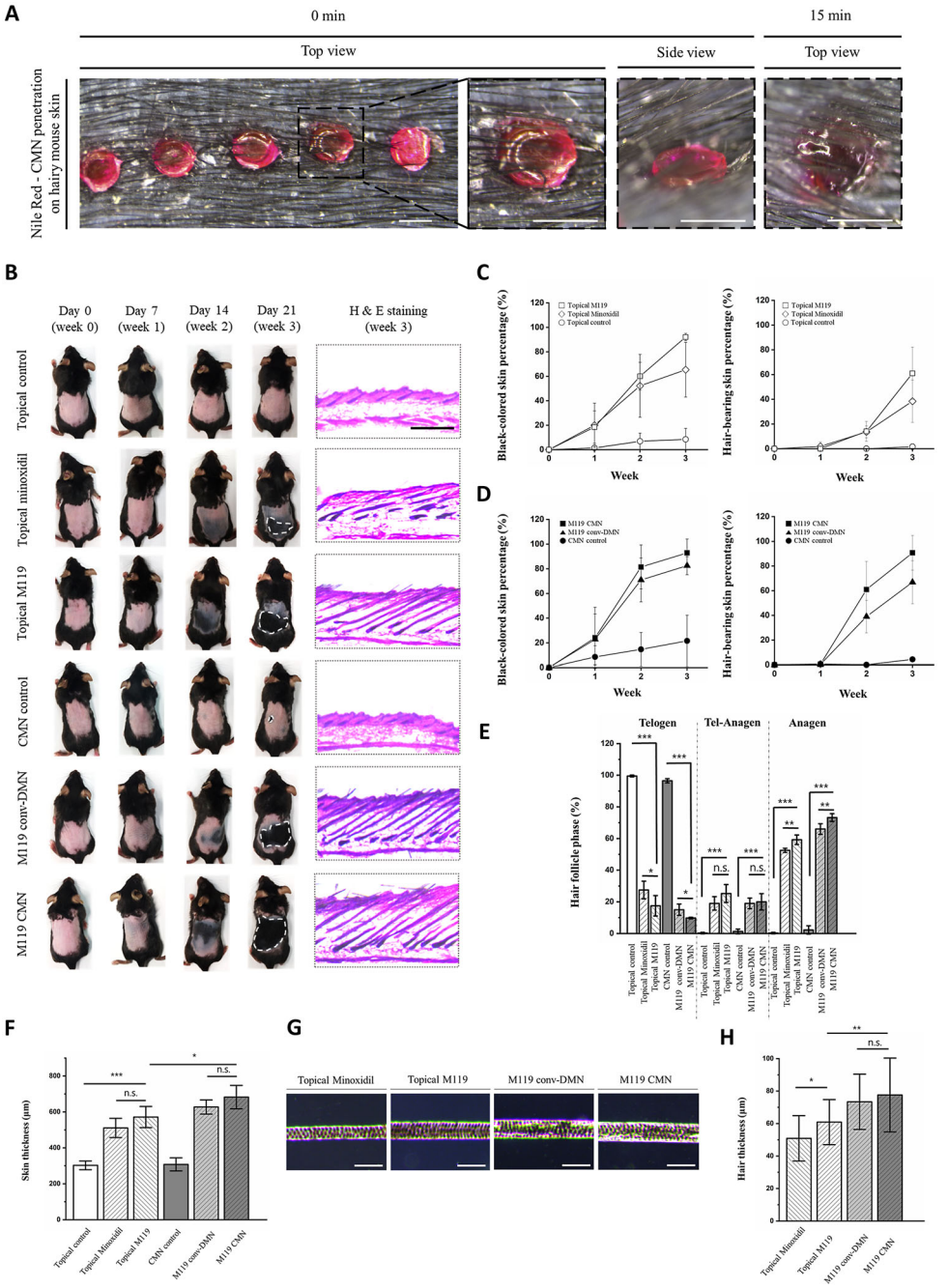

Figure 5. A comparative study for evaluating the hair growth efficacy of M119-loaded CMN. A) Nile red–CMN application on live mice dorsal skin with dense hair shafts for visualization of penetration of CMN into the hairy skin assisted by the applicator. The applicator allowed microneedles to penetrate the hairy skin without patches (scale bar, 500 μm). B) M119-loaded CMN showed entirely covered hair growth pattern in the shaved dorsal skin of mice at day 21. In particular, M119-loaded CMN group showed distinctive hair growth area as compared with the other groups. Black dashed box indicates topical formulations and microneedle groups applied region. White dashed line indicates hair growth region in the shaved skin. Topical minoxidil was selected as positive control. The right images of mice indicate H&E staining of the sectioned dorsal skin at day 21 of each group ($n = 4$) (scale bar, 500 μm). C) Black-colored skin percentage and hair-bearing skin percentage in the shaved dorsal area in the topical formulation groups. Black-colored skin implies the tendency that the skin converged to the anagen phase. D) Black-colored skin percentage and hair-bearing skin percentage in the shaved dorsal area in the microneedle treatment groups. E) Hair follicle telogen-to-anagen conversion rate analyzed by biopsy from mice of each group. F) Skin thickness from epidermis to subcutaneous fat was measured. G) Bright field images of matured hair shafts observed in the four experimental groups. Topical control and CMN control were not chosen because they did not show matured hair shafts of anagen phase (scale bar, 100 μm). H) M119 showed considerable hair thickening effect compared to minoxidil. M119-loaded conv-DMN and M119-loaded CMN promoted hair shaft thickness ($n = 30$). Data are expressed as the mean ± SD. $^*p < 0.05$, $^{**}p < 0.01$, $^{***}p < 0.001$. n.s. means nonsignificant.

was observed in the quantitative in vitro Franz diffusion test, with CMN showing 1.4-fold drug delivery rate compared to conv-DMN (Figure 3E). Consistent with the finding of in vitro test that drug delivery efficacy of CMN in the hypodermic region was higher than that of the conv-DMN, this tendency was overlapped in the hair-bearing region of in vivo test.

Histomorphometric analysis of hair follicle telogen-to-anagen conversion rate (Figure 5E) was analyzed by H&E staining of hair follicles from sectioned skin and distinguished as either in the telogen phase, tel-anagen transition state, or anagen phase. A higher percentage of hair follicles in the anagen state indicated a high potential for hair growth. The morphosis of hair follicles was analyzed based on morphological specificity.[25] The M119-loaded CMN (72.3 ± 2.5%) group showed the highest conversion rate among all experimental groups, followed by M119-loaded conv-DMN (66.0 ± 3.4%), topical M119 (59.3 ± 3.0%), and minoxidil (52.5 ± 1.3%) (Figure 5E). These results could confirm hair induction efficacy of M119-loaded CMN again.

Further, we analyzed the skin thickness (Figure 5F), one of the major factors of hair growth. Although skin thickness after topical M119 application showed significant skin proliferation compared to the topical control group, it was not significantly different from that after topical minoxidil application. Additionally, skin thickness after M119-loaded CMN application (682.5 ± 65 μm) showed significant skin proliferation compared to that after topical M119 application (571.5 ± 58.9 μm), implying that CMN might have induced skin proliferation. Furthermore, we analyzed hair shaft thickness of grown hair of each group ($n = 30$) after biopsy of the topical and microneedle-applied dorsal areas, as shown in Figure 5G and Figure 5H. Although the hair bearing region percentage of M119-loaded CMN was significantly higher than that of M119-loaded conv-DMN, the difference in hair shaft thickness was not significant because we harvested hair shafts from mature hair follicles grown in the dorsal region.

In summary, M119-loaded CMN showed improved hair growth indices such as hair induction efficacy and hair growth compared to conv-DMN and topical formulation, suggesting CMN as a promising platform for alopecia treatment through induction of anagen and hair growth. In next step, we analyzed the cause of these results in protein expression level through immunofluorescence studies.

We evaluated in vivo efficacy of M119 and M119-loaded CMN. To support in vivo data, we validated the expression and distribution of major hair growth-related proteins using immunofluorescence studies that could track protein distribution in tissues with conjugated antibodies targeting β-catenin, PCNA, MECA 32, and versican (VCAN).[26,27] The qualitative and quantitative fluorescence signal intensity of β-catenin and PCNA are shown in **Figure 6**A–C. As shown in Figure 6B, topical M119 (62.0 ± 5.8) showed significant difference from topical minoxidil (56.6 ± 2.7) in β-catenin signal, indicating that M119 induced epithelial growth for supporting hair growth. Interestingly, M119-loaded CMN showed the highest epithelial cell proliferation (72.2± 2.7), whereas it was 66.8 ± 3.3 for M119-loaded conv-DMN. We could infer that the M119 activated the Wnt/β-catenin signaling pathway, which is responsible for regeneration of epithelial tissue.[28] We also analyzed PCNA markers (Figure 6C); surprisingly, the CMN control group (57.0 ± 3.0) showed significant difference in PCNA intensity from the topical M119 group (47.4 ± 3.8), whereas there was no significant difference among the microneedle treatment groups. The superior PCNA intensity trend in microneedle treatment groups might be due to proliferation of epithelial cells to cure the wounds from microneedle pores. This epithelial cell proliferation trend of microneedle treatment groups explained the needling effect.[29] Further, the skin thickening effect (Figure 5E) could be explained by β-catenin signaling and PCNA upregulation caused by microneedle application.

The vascular network around the hair follicles is essential for hair growth because it supplies nutrients to the hair follicles.[30] Developing vascular network in perifollicular region plays a key role in alopecia treatment by relieving hair follicle aging condition and reconstructing hair follicle environment.[31] For visualizing this vascularization, we used the panendothelial marker MECA 32 for tracking the vessels around the hair follicles through fluorescence (Figure 6D) and mean intensity of the vessel marker (Figure 6E). The quantitative fluorescence intensity of topical M119 (55.8 ± 3.6) was higher than that of topical minoxidil (50.5 ± 2.8), indicating more evident vascular network. Further, M119-loaded CMN (68.6 ± 4.4) showed significantly higher intensity than that of M119-loaded conv-DMN (62.2 ± 6.9) and topical M119. This result shows that M119 has superior vasodilating effect compared to the most widely used alopecia drug minoxidil. Along with β-catenin, VCAN present in the dermal papilla is a key target protein in alopecia treatment. VCAN, reported as a specific marker of the dermal papilla, is related to the β-catenin signaling pathway and plays an essential role in DPC aggregative growth, which causes hair induction and growth.[32] VCAN fluorescence in the dermal papilla is described by white dashed line (Figure 6F), and the intensity of VCAN was highest in the M119-loaded CMN group (62.2 ± 6.9), followed by M119-loaded conv-DMN, topical M119, and topical minoxidil, in order (Figure 6G). We excluded topical control and CMN control groups because the anagen-induced hair follicles of the two groups were deficient for analysis (Figure 5D). This strong intensity of dermal papilla VCAN in M119-loaded CMN was due to the targeted delivery of M119 to the hair follicles, which stimulated hair inductive properties of dermal papilla.

The M119-loaded CMN group performed better than the other groups with respect to both vascularization and hair induction, and we could speculate that this performance resulted from the target delivery of CMN to the hair follicles, which stimulated anagen and promoted hair shaft growth. The enhanced vascularization of the hair follicles in this group supplied M119-enriched nutrition and DPC proliferation. Next, upregulation of VCAN expression might have accelerated anagen induction and hair growth. Furthermore, the enhanced hair growth through hair follicle targeting efficacy of the CMN delivery system might be supported by the applicator. These beneficial effects of CMN with the applicator system in alopecia treatment were harmoniously combined with novel M119 drug, which showed distinctive hair growth efficacy.

3. Conclusion

Our study indicates that the novel vasodilator M119 drug is one of the future candidates for the alopecia treatment, and CMN with a newly designed applicator is a key solution for enhancing and targeting drug delivery to the hair follicles. The applicator

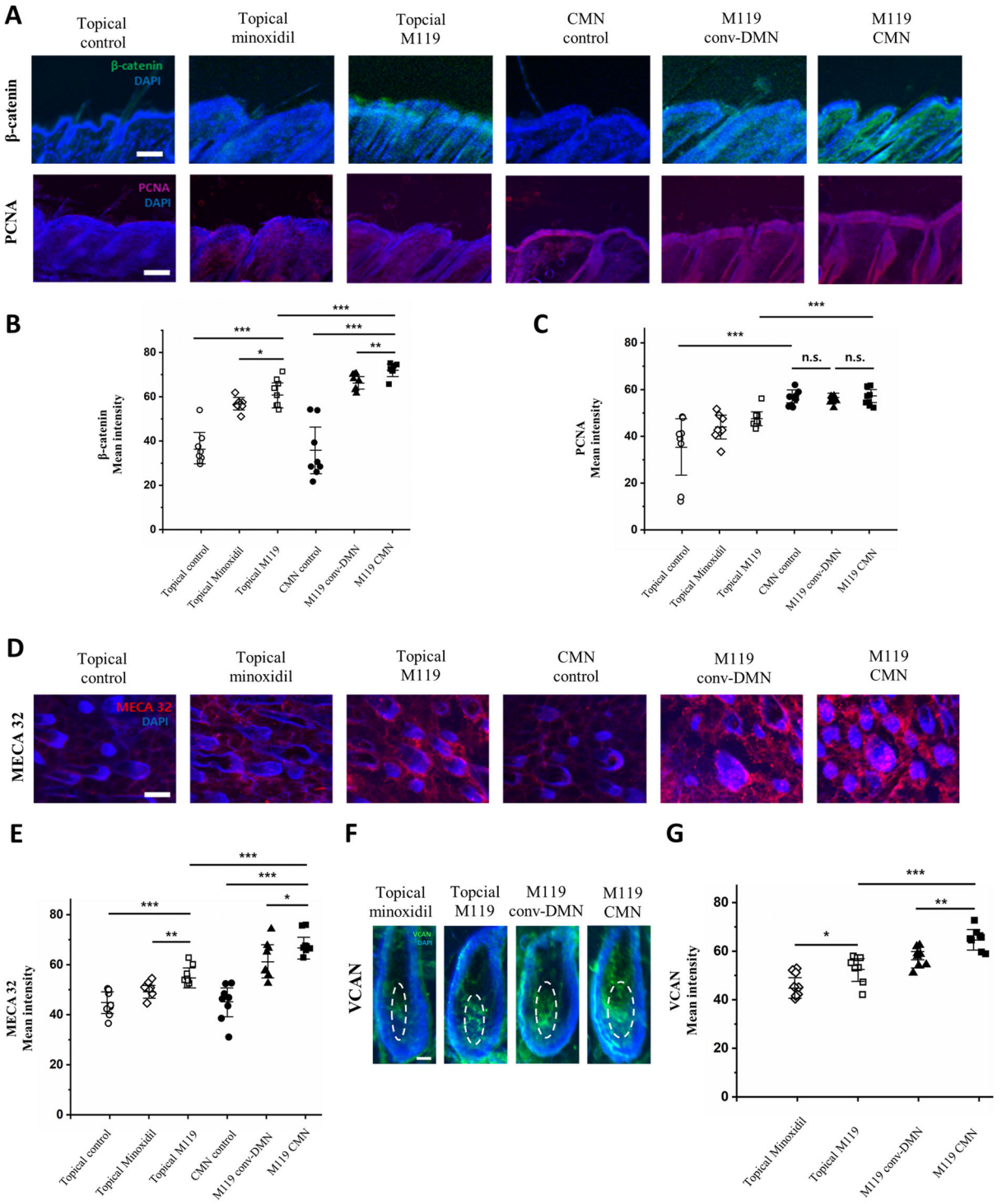

Figure 6. M119-loaded CMN upregulated epithelial proliferation, vascularization around the hair follicles for hair nutrition supply, and dermal papilla hair induction. The protein expression was analyzed by immunofluorescence staining. A) Protein β-catenin was upregulated in both minoxidil and M119 groups. All microneedle treatment groups including CMN control showed higher PCNA expression level than those of the topical formulation groups. The nuclei were stained with DAPI (scale bar, 50 μm). B) β-catenin mean intensity indicates epidermal growth needed for hair growth. C) PCNA mean intensity implies cell proliferation of the skin biopsy. D) Representative image of immunofluorescence staining of MECA 32, a vessel marker targeting panendothelial cell. The red network indicates blood vessels surrounding the hair follicles for hair nutrition supply (scale bar, 50 μm). E) MECA 32 intensity indicates level of vascularization around the hair follicles. F) Representative VCAN expression in hair dermal papilla responsible for hair induction. White dashed line indicates hair dermal papilla. The dermal papilla of topical control and CMN control were not sufficiently developed for analysis (scale bar, 20 μm). G) VCAN mean intensity implies the level of hair induction. Data in (B), (C), (F), and (G) ($n = 8$) are expressed as the mean ± SD. $^*p < 0.05$, $^{**}p < 0.01$, $^{***}p < 0.001$. n.s. means nonsignificant.

overcame the problem of poor insertion of microneedle patches through the use of micropillars. Furthermore, lack of drug delivery to the hypodermic region by conv-DMN was resolved by CMN. Since enhanced drug delivery to the hair follicles in the hypodermic region is required for alopecia treatment, combination of these two advanced technologies is an optimized platform for the alopecia treatment. Additionally, this successful research using vasodilator loading microneedle will open a new prospect in future vasodilator loading microneedle research. In other words, the microneedle may be a potent solution to be utilized in diseases which the vasodilation can be an effective treatment such as erectile dysfunction, cardiovascular disease, wound healing, altitude sickness, skin fibrosis, ophthalmology, medical cosmetics, oncology, lung fibrosis, and diabetic foot disease. In conclusion, our system showed significant hair growth stimulation with vascularization compared to the existing systems for alopecia treatment; thus, an advanced M119-loaded CMN drug delivery system has been suggested as one of the promising candidates for future alopecia specialized treatment.

4. Experimental Section

Fabrication of CMN: CMN was fabricated in two main steps: fabrication of base layer and head layer. The base layer, which was composed of biodegradable polymer, was fabricated using contact-and-dry method. After dispensing 20% w/v of pharmaceutical grade hyaluronic acid aqueous solution (PHA, 30 kDa; Uscarepharm, Suwon, Republic of Korea) on a 4% w/v carboxymethylcellulose (CMC, 90 kDa; Sigma-Aldrich, St. Louis, MO, USA) coated plate, the droplets were placed in contact with a cover plate. The droplet was formed into a sandglass shape by natural drying with a constant 300 μm distance between the two plates. Next, 60% w/v PHA droplets were dispensed on the sandglass-shaped PHA structures. Further, the CMN was fabricated by centrifugal lithography at 202 g force for 1 min. The PHA droplets mentioned above loaded 0.027% w/v of TOP-M119 (M119) (TOPADUR, Zurich, Switzerland) and final M119 CMN fabricated by this solution contained 2 μg (same amount of drug loaded in topical M119 solution and M119 conv-DMN) of M119 drug per 5 × 5 array.[20] Conv-DMN was fabricated using the same polymers, drug loading amount, and height (700 μm) as that of CMN.

Applicator: The microneedle applicator that supports penetration of CMN was designed for application on the scalp, which is a hairy part of the skin. Micropillars in the device were aligned in microneedle arrays, which provided an insertion force for penetrating the hairy skin.

Preparation of Topical Minoxidil and Topical M119 Solutions: Topical formulations and conv-DMN having conical shape loaded with M119 were prepared to compare the efficacy of different alopecia treatments. In the topical formulation, polyethylene glycol 400 (PEG 400; Sigma-Aldrich, St. Louis, MO, USA) and ethanol (99.5°; Sigma-Aldrich) were mixed in 50 μL solution with a ratio of 7:3 v/v containing 2% w/v of minoxidil (Sigma-Aldrich) and 0.002% w/v of M119 (2 μg per day). The topical formulation groups' 50 μL solutions were administered twice a day.

Morphological Characteristics, Penetration Strength, and SEM Analysis: The morphological characteristics of the CMN were analyzed using a bright field microscope (M165 FC; Leica, Wetzlar, Germany). The length and head, base, and tip diameters of the CMN were observed. The mechanical strength of CMN and conv-DMN for skin penetration was analyzed using a force analyzer (Z0.5TN; Zwick/Roell Inc., Ulm, Germany), which recorded the axial force when the sensor was pressed on the CMN in the vertical downward direction at a velocity of 3.6 mm min^{-1}. Microneedle's surface characteristics were observed through SEM data using FE-SEM microscope (IT-500HR; JEOL, Tokyo, Japan).

Skin Penetration Analysis by OCT: The skin penetration ability of the CMN was analyzed using OCT (Kyungpook National University, Daegu, Korea). CMN was applied to the shaved pig cadaver skin (thickness: ≈1.0–1.2 mm; Cronex, Hwaseong, Korea), and real-time investigation was performed without histological sections.

High-Performance Liquid Chromatography (HPLC) Conditions for M119: A reverse-phase HPLC (Waters 600S; Waters, Milford, MA, USA) was used with a C18 column (150 mm × 4.6 i.d., Cosmosil 5C18-AR-II; Nacalai Tesque Inc., Kyoto, Japan) for quantitative analysis of M119 loading amount in CMN. To set a calibration curve, a stock solution of M119 was prepared and the solution was sequentially diluted from 1.5 mg mL^{-1} to 0 ($R^2 \geq 0.99$). A mobile phase was prepared with 50% v/v acetonitrile and 50% v/v distilled water and the flow rate was set at 1 mL min^{-1}. The detection wavelength of M119 was 254 nm. The retention time was determined to be 6.625 min.

Qualitative Diffusion Analysis of CMN in the Pig Cadaver Skin using Nile Red: For diffusion analysis in the porcine skin, Nile red (Sigma-Aldrich, St. Louis, MO, USA) was used as the model drug for the topical, conv-DMN, and CMN groups. The same concentration of Nile red (0.1% w/v) was used in topical solution, conv-DMN, and CMN. Experiments were conducted using Franz diffusion cell (Hanson, Chatsworth, CA, USA) for 24 h to simulate the actual application. After 24 h, the skin samples that were subjected to diffusion test were washed with distilled water and dried. The Nile red fluorescence was analyzed using the fluorescent mode of M165 FC microscope (Leica), and the signal intensity was measured using the ImageJ software (National Institutes of Health, Bethesda, MD, USA). The bottom view of the skin (opposite site of application of topical solutions and needles) was analyzed to visualize lateral drug diffusion. In addition, cross-sections of each skin were imaged to visualize vertical drug diffusion under 700 μm region. The cross-sectioned samples were sectioned vertically to the surface of the skin after freezing at −4 °C for 30 min.

Quantitative Diffusion Analysis of CMN in the Porcine Skin using Nile red: To support qualitative diffusion data, a quantitative cumulative release analysis of Nile red-loaded topical, conv-DMN, and CMN groups was conducted using Franz diffusion cell test kit. In the topical group, 100 μL solution was applied in an area of 2 × 2 cm^2 of the porcine skin. In the conv-DMN and CMN, 25 microneedles (5 × 5 arrays) were applied each in an area of 2 × 2 cm^2 of the porcine skin using a microneedle applicator. Each experiment was conducted five times. A receptor fluid, which consisted of phosphate-buffered saline (PBS, Life Technologies, Eugene, OR, USA) and 20% v/v ethanol, was maintained at 32 °C using a water jacket.[6] 1 mL of the samples at fixed intervals of 0, 1, 2, 4, 8, 24, and 48 h were analyzed. Nile red quantification was performed by UV-VIS spectroscopy at a wavelength of 559 nm, with positive control solution for each sample that dissolved Nile red-loaded topical solution, conv-DMN, and CMN in the same volume of Franz cell receptor solution.

Cell-Free Enzymatic PDE5A Activity Assay: The inhibition of recombinant human PDE5A1 (Sigma Aldrich AG, Buchs, Switzerland) by test or reference items was measured in a radiometric assay based on Scintillation Proximity Assay (SPA) technology as previously described with modifications.[33] The enzyme activity assay was performed in 20 × 10^{-3} M Tris HCl pH 7.4, 5 × 10^{-3} M $MgCl_2$, 0.01% bovine serum albumin, and 0.5 × 10^{-6} M cGMP/[^{3}H] cGMP substrate. The incubation was initiated by addition of substrate following a preincubation for 10 min of the PDE5A1 enzyme with test or reference items or vehicle. The hydrolysis of [^{3}H]cGMP/cGMP by PDE5A1 was terminated by adding SPA beads (RPNQ0024, Perkin Elmer, Waltham, MA) at a volume of 50 μL per well, prediluted in water according to the manufacturer´s instructions and supplemented with 3-isobutyl-1-methylxanthine (3 × 10^{-3} M). Beads were allowed to sediment for at least 30 min before measurement in a Wallac Microbeta 2 (Perkin Elmer). The numbers of experiment for each group were sildenafil ($n = 15$), M119 ($n = 4$), first metabolite ($n = 4$), and second metabolite ($n = 5$). Percent inhibition values compared to vehicle control were calculated and IC50 values were computed by GraphPad Prism 8.2.0 software with nonlinear regression using the sigmoidal dose–response function. Results were given as the mean from *N* independent experiments each performed in triplicate.

cGMP Enzyme-Linked Immunosorbent Assay (ELISA): Isolation of human platelets and incubations for measurements of total cGMP were performed as previously described with modifications.[33] Platelets were

isolated from human buffy coats negatively tested for human immunodeficiency virus, hepatitis B virus, and hepatitis C virus, acquired from the Zurich Red Cross Blood Donation Service (Schlieren, Switzerland). Buffy coats were diluted 3.2-fold v/v in 150×10^{-3} M NaCl, 34.8×10^{-3} M sodium citrate, and centrifuged at $200 \times g$ for 10 min. Next, 9 volumes of the resulting platelet rich plasma were supplemented with 1 volume of 85×10^{-3} M sodium citrate, 111×10^{-3} M D-glucose, 71×10^{-3} M citric acid, and apyrase (2 U mL^{-1} final concentration, #A6410, Sigma-Aldrich). Following centrifugation at $1400 \times g$ for 10 min, platelets were carefully resuspended in Tyrode (134×10^{-3} M NaCl, 12×10^{-3} M $NaHCO_3$, 2.9×10^{-3} M KCl, 0.36×10^{-3} M NaH_2PO_4, 5×10^{-3} M HEPES, 5×10^{-3} M D-Glucose, pH 7.4) at a density of 9×10^8 cells mL^{-1}. Washed platelets (final concentration 4.5×10^8 cells mL^{-1}) were preincubated for 30 min with the soluble guanylate cyclase stimulator riociguat (1×10^{-6} M, #HY-14779, Lucerna Chem AG, Lucerne LU, Switzerland) and the selective PDE2 inhibitor BAY 60–7550 (100×10^{-9} M, HY#14-992, Lucerna Chem AG, Lucerne LU, Switzerland) before M119 or sildenafil (both in serial dilutions from 1×10^{-9} M to 10×10^{-6} M, half-logarithmic steps), or vehicle were added to a final volume of 200 µL. Vehicle (0.3% dimethyl sulfoxide (DMSO)) was identical in all wells. Following a 2 h incubation time, 20 µL 2N HCl was added. Supernatants from a 5 min $1000 \times g$ centrifugation step were frozen at −80 °C. Total platelet cGMP (pmol mL^{-1}) content was determined using a commercially available ELISA (Direct cGMP ELISA, ADI-901-014, Enzo Life Sciences ELS, Lausen BL, Switzerland), following the instructions of the manufacturers.

hDPCs Culture and Reagents: Primary human dermal papilla cells (hDPCs) at passages 2–7 were used in this study. The cells were cultured in low-glucose Dulbecco's modified Eagle medium (DMEM, Hyclone, Pittsburgh, USA) supplemented with 10% fetal bovine serum (Gibco, Gaithersburgh, USA), 1% antibiotic-antimycotic (Gibco), 1 ng mL^{-1} bFGF (Peprotech, Princeton, USA), and 5 µg mL^{-1} insulin (Gibco) at 37 °C in a 5% CO_2 humidified atmosphere.

Cell Viability Analysis: The hDPCs were seeded in 24-well plates and treated with DMSO vehicle, 100×10^{-6} M minoxidil, and 30×10^{-9} M M119 for 24 h. Cell viability was measured using the CellTiter-Glo Luminescent Cell Viability Assay Kit (Promega, Madison, USA) following the manufacturer's instructions. The luminescent activities were observed using FLUOstar OPTIMA luminometer (BMG Labtech, Offenburg, Germany).

Quantitative Real-Time PCR: The hDPCs were seeded at a density of 3×10^5 cells per well in 6-well plates and treated with M119 (30×10^{-9} M) for 48 h. The cells were washed with PBS, and RNA was isolated using TRIzol reagent (Invitrogen, Massachusetts, USA) following the manufacturer's instructions. Total RNA (2 µg) was reverse-transcribed using 200 units of reverse transcriptase (Invitrogen) in 40 µL reaction mixture at 42 °C for 1 h. The cDNA (2 µL) was amplified to 40 µL reaction mixture containing 10×10^{-3} M dNTP (Takara, CA, USA), 10 pmol primer set (Bioneer, Daejeon, Korea), and 1 U Taq polymerase (Invitrogen). The following primers were used: VEGF, forward 5'-ACT TCT GGG CTG TTC TCG-3' and reverse 5'-TCC TCT TCC TTC TCT TC-3'; β-actin, forward 5'-AGAGCTACGAGCTGCCTGAC-3' and reverse 5'-AGC ACT GTG TTG GCG TAC AG-3'.

Western Blot Analysis: The cells were washed with PBS and lysed with radioimmunoprecipitation assay buffer. The lysates were centrifuged at $16\,000 \times g$ at 4 °C for 30 min. Each protein (20 µg) was separated on 8–10% sodium dodecyl sulfate–polyacrylamide gel electrophoresis gel and transferred to nitrocellulose membrane (Schleicher & Schuell Co., Keene, USA) and used as a molecular weight marker. After blocking with 5% skim milk for 1 h at room temperature, membranes were blotted overnight at 4 °C with the following primary antibodies: mouse anti-α-tubulin (Cell Signaling Technology Cat# 3873, 1:4000, Danvers, USA) and mouse anti-PCNA (Santa Cruz Biotechnology Cat# sc-56, 1:500, Dallas, USA). The membranes were blotted with HRP-conjugated anti-mouse IgG secondary antibodies. The antibody dilutions were reused five times and maintained under −20 °C condition. The blots were visualized using chemiluminescence (Amersham Biosciences, Buckinghamshire, UK) and LAS-4000 image analyzer (Fujifilm, Tokyo, Japan).

Ex Vivo Vibrissa Organ Culture: Mouse vibrissa anagen follicles were isolated from C57BL/6 mice for organ culture. The isolated vibrissa follicles were cultured in 500 µL DMEM supplemented with 100 U mL^{-1} penicillin/streptomycin (Gibco, Gaithersburgh, USA), and 12.5 µg mL^{-1} gentamicin (Gibco, Gaithersburgh, USA) in 24-well plates. The vibrissa follicles were treated with DMSO, 100×10^{-6} M minoxidil, 3×10^{-9} M M119, and 30×10^{-9} M M119, and cultured for 6 days. The medium was changed every 2 days.

Animals and Ethical Approval: Animal experiments were conducted following the ethical guidelines and regulations at the Yonsei Laboratory Animal Research Center (YLARC). All procedures were approved by the Institutional Animal Care and Use Committee (IACUC) of the Yonsei University (Approval number: IACUC-202012-1189-02). Female C57BL/6 mice (6 weeks old) were purchased from Orient Bio (Seongnam, Korea) and allowed to adapt for 1 week. 7 weeks old mice in the telogen phase were shaved with a clipper to expose the dorsal skin area. The mice were treated with topical control solution, void CMN (CMN control), topical minoxidil, topical M119, M119-loaded conv-DMN, and M119-loaded CMN for 21 days ($n = 4$ per group). The topical groups were treated twice daily, and the microneedle treatment groups were treated once every alternate day. All mice were housed at room temperature (22–24 °C) with a 12 h light/dark cycle.

Histological and Immunofluorescence Staining: Mouse skin tissues were isolated from the dorsal area and fixed overnight in 4% w/v paraformaldehyde (Sigma-Aldrich). The fixed tissues were dehydrated and embedded in an optimal cutting temperature compound (Leica). The tissues were then cryo-sectioned into 10 µm thick slices. The sectioned slices were stained with hematoxylin for 3 min and eosin for 30 s (H&E staining) and imaged using M165 FC microscope (Leica). For immunofluorescence staining, the cryo-sectioned tissues of each experimental group were treated with 0.5% w/v Trion-X 100 (MP biomedicals, OH, USA) to enhance cell permeation of antibody and blocked in 5% w/v normal mouse serum for 30 min. The following conjugated antibodies were used to target β-catenin (BD Biosciences, San Jose, CA, USA), PCNA (LSBIO, Seattle, WA, USA), VCAN (LSBIO, Seattle, WA, USA), and MECA 32 (Novus Biologicals, CA, USA). The antibodies were labeled with the molecular probes Alexa Fluor 488, DY-550, FITC, and Allophycocyanin, respectively. After treatment with antibodies, the sections were incubated overnight at 4 °C. 4'6-diamidino-2-phenylindole (DAPI) was used as the mounting medium for counterstaining. The fluorescence data were obtained by the fluorescent mode of M165 FC microscope (Leica), and the intensity was measured using the ImageJ software (National Institutes of Health).

Statistical Analysis: Data were expressed as the means were compared using Student's *t*-test or one-way analysis of variance (ANOVA) using the GraphPad Prism 6.0 and 8.2.0 software (GraphPad Software Inc.). The results were obtained from four or more groups. Statistical significance was set at $p \leq 0.05$.

Supporting Information

Supporting Information is available from the Wiley Online Library or from the author.

Acknowledgements

This work was supported by the National Research Foundation of Korea (NRF) grant funded by the Korean government (MSIT) (grant number: 2020M3E5D8108104), a grant of the Korea Health Technology R&D Project through the Korea Health Industry Development Institute (KHIDI), funded by the Ministry of Health & Welfare, Republic of Korea (grant number: HI20C1234), and the Brain Korea 21(BK21) FOUR program. Dr. Hermann Tenor, Esra Lone, and Jaan Strang (TOPADUR Pharma AG) for the PDE activity assay and cGMP measurements in human platelets are thanked.

Conflict of Interest

Y.K., P.A., R.d.B.F, R.N., and H.J. are inventors of TOP-M119 microneedle's patent. TOPADUR pharma AG, Yonsei University, and JUVIC have

the patent right. This potential conflict of interest has been disclosed and is managed by TOPADUR, Yonsei University and JUVIC together.

Data Availability Statement

The data that support the findings of this study are available from the corresponding author upon reasonable request.

Keywords

alopecia, microneedle, microneedle applicator, transdermal drug delivery, vasodilator new drug candidate

Received: March 11, 2022
Revised: May 3, 2022
Published online: May 25, 2022

[1] K. J. McElwee, J. Shapiro, *Skin Ther. Lett.* **2012**, *17*, 1.
[2] D. Monti, S. Tampucci, S. Burgalassi, P. Chetoni, C. Lenzi, A. Pirone, F. Mailland, *J. Pharm. Sci.* **2014**, *103*, 2307.
[3] A. K. Ali, B. S. Heran, M. Etminan, *Pharmacotherapy* **2015**, *35*, 687.
[4] M. S. Irwig, *Dermatology* **2020**, *236*, 540.
[5] D.-D. Nguyen, M. Marchese, E. B. Cone, M. Paciotti, S. Basaria, N. Bhojani, Q.-D. Trinh, *JAMA Dermatol.* **2021**, *157*, 35.
[6] S. Kim, J. Eum, H. Yang, H. Jung, *J. Controlled Release* **2019**, *316*, 1.
[7] C. Jahoda, K. Horne, R. Oliver, *Nature* **1984**, *311*, 560.
[8] H. Hori, G. Moretti, A. Rebora, F. Crovato, *J. Invest. Dermatol.* **1972**, *58*, 396.
[9] N. Orentreich, H. M. Strum, A. I. Weidman, A. Pelzig, *Arch. Dermatol.* **1960**, *82*, 894.
[10] J. Ohn, M. Jang, B. M. Kang, H. Yang, J. T. Hong, K. H. Kim, O. Kwon, H. Jung, *Adv. Sci.* **2021**, *8*, 2004873.
[11] M. R. Prausnitz, *Adv. Drug Delivery Rev.* **2004**, *56*, 581.
[12] J. W. Lee, S. O. Choi, E. I. Felner, M. R. Prausnitz, *Small* **2011**, *7*, 531.
[13] R. Fertig, A. Gamret, J. Cervantes, A. Tosti, *J. Eur. Acad. Dermatol. Venereol.* **2018**, *32*, 564.
[14] I.-J. Choi, W. Na, A. Kang, M.-H. Ahn, M. Yeom, H.-O. Kim, J.-W. Lim, S.-O. Choi, S.-K. Baek, D. Song, *Eur. J. Pharm. Biopharm.* **2020**, *153*, 150.
[15] E. Larrañeta, J. Moore, E. M. Vicente-Pérez, P. González-Vázquez, R. Lutton, A. D. Woolfson, R. F. Donnelly, *Int. J. Pharm.* **2014**, *472*, 65.
[16] H.-R. Jeong, H.-S. Lee, I.-J. Choi, J.-H. Park, *J. Drug Targeting* **2017**, *25*, 29.
[17] S. F. Lahiji, Y. Kim, G. Kang, S. Kim, S. Lee, H. Jung, *Sci. Rep.* **2019**, *9*, 7886.
[18] K. E. Andersson, *Br. J. Pharmacol.* **2018**, *175*, 2554.
[19] Y. C. Ryu, D. H. Lee, J. Shim, J. Park, Y. R. Kim, S. Choi, S. S. Bak, Y. K. Sung, S. H. Lee, K. Y. Choi, *Br. J. Pharmacol.* **2021**, *178*, 2533.
[20] G. Yang, Q. Chen, D. Wen, Z. Chen, J. Wang, G. Chen, Z. Wang, X. Zhang, Y. Zhang, Q. Hu, *ACS Nano* **2019**, *13*, 4354.
[21] H. Yang, S. Kim, G. Kang, S. F. Lahiji, M. Jang, Y. M. Kim, J. M. Kim, S. N. Cho, H. Jung, *Adv. Healthcare Mater.* **2017**, *6*, 1700326.
[22] X. Ning, C. Wiraja, D. C. S. Lio, C. Xu, *Adv. Healthcare Mater.* **2020**, *9*, 2000147.
[23] M. K. Dymond, G. S. Attard, *Langmuir* **2008**, *24*, 11743.
[24] K. Yano, L. F. Brown, M. Detmar, *J. Clin. Invest.* **2001**, *107*, 409.
[25] S. Müller-Röver, K. Foitzik, R. Paus, B. Handjiski, C. van der Veen, S. Eichmüller, I. A. McKay, K. S. Stenn, *J. Invest. Dermatol.* **2001**, *117*, 3.
[26] H.-I. Choi, B.-M. Kang, J. Jang, S. T. Hwang, O. Kwon, *Biochem. Biophys. Res. Commun.* **2018**, *505*, 685.
[27] E. R. Deschene, P. Myung, P. Rompolas, G. Zito, T. Y. Sun, M. M. Taketo, I. Saotome, V. Greco, *Science* **2014**, *343*, 1353.
[28] Y. Yang, Y. Li, Y. Wang, J. Wu, G. Yang, T. Yang, Y. Gao, Y. Lu, *J. Dermatol. Sci.* **2012**, *68*, 157.
[29] Y. S. Kim, K. H. Jeong, J. E. Kim, Y. J. Woo, B. J. Kim, H. Kang, *Ann. Dermatol.* **2016**, *28*, 586.
[30] M. Semalty, A. Semalty, G. P. Joshi, M. S. M. Rawat, *J. Dermatol. Treat.* **2011**, *22*, 123.
[31] A. Yuan, F. Xia, Q. Bian, H. Wu, Y. Gu, T. Wang, R. Wang, L. Huang, Q. Huang, Y. Rao, D. Ling, F. Li, J. Gao, *ACS Nano* **2021**, *15*, 13759.
[32] E. Taghiabadi, M. A. Nilforoushzadeh, N. Aghdami, *Skin Pharmacol. Physiol.* **2020**, *33*, 280.
[33] M. B.-Y. Greenwald, C. Tacconi, M. Jukic, N. Joshi, P. Hiebert, J. Brinckmann, H. Tenor, R. Naef, S. Werner, *J. Invest. Dermatol.* **2021**, *141*, 415.

